



# Turbulence modeling of rotating confined flows

Laurent Elena and Roland Schiestel

Institut de Recherche sur les Phénomènes Hors d'Equilibre, Département Modélisation Numérique, Marseille, France

We propose here an original differential stress model which takes into account some of the implicit effects of rotation on the turbulence. It is applied to the numerical prediction of the turbulent flow inside a shrouded rotor-stator system. The results of this model are compared to those obtained with four other turbulence models and to the experimental data. The advanced second-order models produce quite correct predictions for the mean flow, but it is shown that it is necessary to take account of the rotation effects in order to obtain satisfactory behaviour of the Reynolds stress.

**Keywords:** turbulence modeling; rotation; turbulent flow

## Introduction

Numerical prediction of the turbulent flow in rotating cavities is of crucial importance for the conception and design in turbomachinery. Indeed, due to the high temperatures, the strong rotation rate, and the complicated geometry, the experiments generally do not allow precise description of the flow inside the cavities of the gas-turbine engine. Thus, the numerical approach seems to be necessary to optimize the cooling system and the geometry; but a turbulence model able to predict a wide range of confined rotating flows accurately remains a difficult challenge.

The aim of this work is to test classical turbulence modeling and to propose improved models for numerical prediction of the inhomogeneous turbulent flow submitted to rapid rotation. More precisely, we consider here the turbulent flow in the shrouded rotor-stator system (see Figure 1) studied experimentally by Itoh et al. (1990). This experiment is a major reference, because the authors produced measurements of not only the mean flow but also of all the six Reynolds-stress components. The authors emphasize the existence of a relaminarized region (near the rotation axis) even for high rotation rates. Consequently, the model must be able to describe the low Reynolds number region not only near a wall but also in the core of the flow. Moreover, the model must accurately predict the location of the transition from laminar to turbulent regime.

The Coriolis forces deeply modify the structure of the turbulence field. Their effects, such as angular dispersion, the tendency of the turbulence to become bidimensional, and the reduction of the dissipation rate  $\varepsilon$ , are underlying subtle interactions and require refined modeling. Thus, we propose a new differential stress model which takes into account these effects. This model is inspired from Reynolds (1991), Reynolds and Kassinos

(1994), and Cambon et al. (1992). Furthermore, the combined effects of confinement and rotation are also taken into account through nonhomogeneous terms in an original manner.

## Turbulence modeling

### Classical models

The models proposed in this work are compared to the more usual ones. We retained for comparisons three turbulence models usually considered to be the standards:

- (1) the low-Reynolds number  $k$ - $\varepsilon$  model of Launder and Sharma (1974);
- (2) a zonal modeling with an algebraic stress model (ASM) in the core of the flow based on the Rodi's hypothesis and a low Reynolds number  $k$ - $\varepsilon$  model for the wall treatment; and
- (3) a classical differential stress model (RSM1) which allows us to compute the low Reynolds number region: the model of Hanjalic and Launder (1976).

For brevity, these three models are not detailed here. Further applications to rotating cavities can be found in Schiestel et al. (1993) and Elena and Schiestel (1995a).

### RSM2 model

The models of the new generation were developed with constant attention to such extreme states of turbulence as the two-component limit near a wall and the strong anisotropies satisfying realisability. Here, we retained the model developed in Launder and Tselepidakis (1994) devised for more general applications.

A few adjustments were necessary to apply this model to the case considered here, where a relaminarized region can develop away from the wall. We specify only the particular forms used for the "slow" part  $\phi_{ij}^{(1)}$  of the pressure-strain correlation and for the dissipation tensor  $\varepsilon_{ij}$ . All the remaining unknown correlations are modeled as in Launder and Tselepidakis (1994).

For  $\phi_{ij}^{(1)}$ , the modeling functions  $\tilde{c}_i$  and  $c'_i$  adopted here are deduced from the Craft's (1991) high Reynolds number proposals

---

Address reprint requests to Dr. R. Schiestel, Modélisation Numérique, Institut de Recherche sur les Phénomènes Hors d'Equilibre, 1 rue Honnorat, 13003 Marseille, France.

Received 2 December 1995; accepted 29 February, 1996

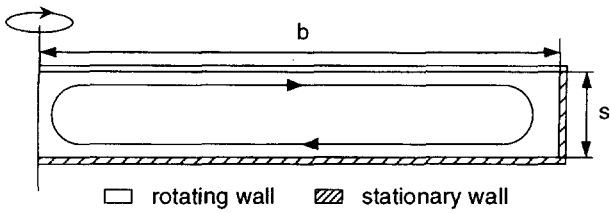


Figure 1 Geometry of the cavity,  $G = s/b = 0.08$

adapted for wall treatment, because they must vanish at the wall.

$$\phi_{ij}^{(1)} = -[\tilde{c}_1 a_{ij}^R + c'_1 (a_{ik}^R a_{kj}^R - \frac{1}{3} A_2^R \delta_{ij})] \varepsilon$$

with

$$\tilde{c}_1 = (3.1 \sqrt{AA_2^R} + 1) [1 - \exp(-Re_t^2/40)]$$

$$c'_1 = 3.72 \sqrt{AA_2^R} [1 - \exp(-Re_t^2/40)] \quad (1)$$

The second-order tensor  $a_{ij}$  denotes the stress anisotropy tensor,  $A_2^R$  and  $A_3^R$  the second and the third invariant of  $a_{ij}$ , and  $A$  is the Lumley's "flatness" parameter  $A = 1 - \frac{9}{8}(A_2^R - A_3^R)$ .

The behaviour of the dissipation tensor at the wall can be obtained by Taylor series of the fluctuating velocity (Launder and Reynolds 1993):

$$\frac{\varepsilon_{11}}{R_{11}} = \frac{\varepsilon_{22}}{4R_{22}} = \frac{\varepsilon_{33}}{R_{33}} = \frac{\varepsilon_{12}}{2R_{12}} = \frac{\varepsilon_{23}}{2R_{23}} = \frac{\varepsilon_{31}}{R_{31}} = \frac{\varepsilon}{k}$$

for the wall  $x_1 = x_3 = 0$ . Away from the wall, it is usual to consider that  $\varepsilon_{ij}$  is isotropic for high Reynolds number of turbulence and should gradually change to  $\varepsilon R_{ij}/k$  as the Reynolds number diminishes. The formulation used here has compliance

with these limits:

$$\varepsilon_{ij} = f_A \varepsilon_{ij}^* + (1 - f_A) \left( f_s \frac{R_{ij}}{k} + \frac{2}{3} (1 - f_s) \delta_{ij} \right) \varepsilon \quad (2)$$

with

$$\varepsilon_{ij}^* = \frac{\varepsilon}{k} \frac{R_{ij} + R_{ik} n_i n_k + R_{kj} n_i n_k + R_{kl} n_k n_l n_i n_j}{1 + \frac{3}{2} (R_{pq}/k) n_p n_q}$$

$$f_A = \exp(-20A^2) \exp(-Re_t^2/20)$$

$$f_s = \exp(-Re_t^2/20)$$

The complete mathematical statement of the RSM2 model is given in Table 1.

### RSM3 model

We propose a model for the spectral tensor  $\Phi_{ij}(\kappa)$  which is developed as a function of the wave vector  $\kappa_i$ , of the classical anisotropy tensor (of the Reynolds stress tensor) and of the directional anisotropy based on the dimensionality tensor:

$$\lambda_{ij}(\kappa) = \oint_{S(\kappa)} \left[ \frac{\kappa_i \kappa_j}{\kappa^2} \Phi_{pp}(\kappa) \right] dS \quad (3)$$

where  $S(\kappa)$  is the sphere of radius  $\kappa$  (Schiestel 1994).

The linear part of the pressure-strain correlation  $\phi_{ij}^{(2)}$  can be derived from this spectral tensor. The resulting form depends on the dimensionality tensor in the physical space

$$\left( C_{ij} = \int_0^\infty \lambda_{ij}(\kappa) d\kappa \right)$$

$$\phi_{ij}^{(2)} = \text{classical terms}$$

$$-0.6 \left( D_{ij}^C - \frac{1}{3} D_{ii}^C \delta_{ij} \right)$$

$$-0.4k(U_{i,j} + U_{j,i}) \quad (4)$$

Notation		
$A$	anisotropy parameter, $A = 1 - \frac{9}{8}(A_2^R - A_3^R)$	$Ro_t$ turbulence Rossby number, $Ro_t = \varepsilon/k\Omega^*$
$a_{ij}^R$	dimensionless anisotropy stress tensor, $a_{ij}^R = R_{ij}/k - 2/3\delta_{ij}$	$U_i$ mean absolute velocity vector
$A_2^R, A_3^R$	second and third stress-anisotropy invariants, $A_2^R = a_{ij}^R a_{ji}^R, A_3^R = a_{ij}^R a_{jk}^R a_{ki}^R$	$U_r, U_\theta, U_z$ radial, tangential, and axial components of the mean velocity in an absolute frame of reference
$a_{ij}^C$	anisotropy of the dimensionality tensor, $a_{ij}^C = C_{ij}/k - 2/3\delta_{ij}$	$\mathbf{n}_i, \mathbf{y}_l$ unit vector normal and distance to the wall
$A_2^C, A_3^C$	second and third $a_{ij}^C$ invariants, $A_2^C = a_{ij}^C a_{ji}^C, A_3^C = a_{ij}^C a_{jk}^C a_{ki}^C$	<b>Greek</b>
$b, s$	disk radius and axial width of the cavity	$\varepsilon$ dissipation rate of turbulent kinetic energy
$C_{ij}$	dimensionality tensor	$\varepsilon_{ij}$ dissipation rate of Reynolds stress tensor
$D_{ij}^R$	$D_{ij}^R = -R_{ik} U_{k,j} - R_{jk} U_{k,i}$	$\varepsilon_{ijk}$ orientation tensor (equal to +1 if indices are all different and cyclic, -1 if different and anti-cyclic, and 0 otherwise)
$D_{ij}^C$	$D_{ij}^C = -C_{ik} U_{k,j} - C_{jk} U_{k,i}$	$\nu$ kinematic viscosity
$D_{ij}^v, D_{ij}^T$	viscous and turbulent diffusion	$\tau_s, \tau_r$ wall shear stress on the stationary and rotating disks
$k$	turbulent kinetic energy	$\phi_{ij}^{(1)}, \phi_{ij}^{(2)}, \phi_{ij}^{(w)}$ turbulence, mean strain, and wall reflection parts of the pressure-strain correlation
$P_{ij}$	Reynolds stress generation by mean shear	$\Omega$ Angular velocity of the disk
$(r, \theta, z)$	radial, tangential, and axial coordinates	$\mathbf{\Omega}$ Rotation vector $\mathbf{\Omega} = (\Omega_1, \Omega_2, \Omega_3)$
$R_{ij}$	Reynolds stress tensor	$\mathbf{\Omega}_i^*$ Intrinsic rotation vector, $\mathbf{\Omega}_i^* = \Omega_i - \frac{1}{2} \varepsilon_{ijk} U_{j,k}$
$Re$	rotational Reynolds number, $Re = \Omega b^2/\nu$	
$Re_t$	turbulence Reynolds number, $Re_t = k^2/\nu\varepsilon$	

**Table 1** RSM2 model for low Reynolds number flows

$$\frac{dR_{ij}}{dt} = P_{ij} + \phi_{ij}^{(1)} + \phi_{ij}^{(2)} + \phi_{ij}^{(2w)} + D_{ij}^T + D_{ij}^v - \varepsilon_{ij}$$

$$P_{ij} = -R_{ik}U_{j,k} - R_{jk}U_{i,k}$$

$$\phi_{ij}^{(1)} = -\left[\tilde{c}_1 a_{ij}^R + c'_1 \left(a_{ik}^R a_{kj}^R - \frac{1}{3} A_2^R \delta_{ij}\right)\right] \varepsilon$$

$$\phi_{ij}^{(2)} = -0.6 \left(P_{ij} - \frac{2}{3} P \delta_{ij}\right) + 0.3 a_{ij}^R P_{ii}$$

$$- 0.2 \left[\frac{R_{kj} R_{ii}}{k} (U_{k,i} + U_{i,k}) - \frac{R_{ik}}{k} (R_{ik} U_{j,i} + R_{jk} U_{i,i})\right]$$

$$- \min(0.6, A) [A_2^R (P_{ij} - D_{ij}^R) + 3 a_{mi}^R a_{nj}^R (P_{mn} - D_{mn}^R)]$$

$$\phi_{ij}^{(2w)} = 0.2 \left(\phi_{km}^{(2)} n_k n_m \delta_{ij} - \frac{3}{2} \phi_{ik}^{(2)} n_k n_j - \frac{3}{2} \phi_{kj}^{(2)} n_i n_k\right)$$

$$\times \frac{k(R_{pq} n_p n_q)^{1/2}}{\varepsilon \gamma}$$

$$D_{ij}^T = 0.22 \left(\frac{k}{\varepsilon} R_{ki} R_{ij,i}\right)_{,k}$$

$$D_{ij}^v = \nu R_{ij,ii}$$

$$\varepsilon_{ij} = f_A \varepsilon_{ij}^* + (1 - f_A) \left(f_s \frac{R_{ij}}{k} + \frac{2}{3} (1 - f_s) \delta_{ij}\right) \varepsilon$$

$$\varepsilon_{ij}^* = \frac{R_{ij} + R_{ik} n_j n_k + R_{kj} n_i n_k + R_{kl} n_k n_l n_i n_j}{1 + \frac{3}{2} (R_{pq}/k) n_p n_q} \frac{\varepsilon}{k}$$

$$\tilde{c}_1 = (3.1 \sqrt{AA_2^R} + 1)(1 - \exp(-\text{Re}_t^2/40))$$

$$c'_1 = 3.72 \sqrt{AA_2^R} (1 - \exp(-\text{Re}_t^2/40))$$

$$f_A = \exp(-20A^2) \exp(-\text{Re}_t^2/20) \quad f_s = \exp(-\text{Re}_t^2/20)$$

where

$$D_{ij}^C = -C_{ip} U_{p,j} - C_{jp} U_{p,i}$$

As a first approach, the tensor  $C_{ij}$  is obtained from a simplified algebraic model deduced from its transport equation:

$$C_{ij} = \frac{2}{3} \left(1 + \frac{f_C}{2}\right) k \delta_{ij} - f_C k \frac{\Omega_i^* \Omega_j^*}{\Omega^{*2}} \quad (5)$$

with the empirical coefficient:

$$f_C = \text{Ro}_t^{-1} / (5 + \text{Ro}_t^{-1})$$

where  $\Omega_i^*$  is the intrinsic rotation vector and  $\text{Ro}_t = \varepsilon/k\Omega^*$ .

Reynolds and Kassinos (1994) have shown that, under rapid mean rotation, the velocity spectrum tensor, due to phase scrambling, approaches a random spectrum:

$$\Phi_{ij}(\mathbf{\kappa}) = \frac{1}{2} \Phi_{ii}(\mathbf{\kappa}) \left(\delta_{ij} - \frac{\kappa_i \kappa_j}{\kappa^2}\right) \quad (6)$$

To enforce this tendency (the model is already compatible to this limit), it is probably beneficial to add an extra source term

$\mathcal{B}_{ij}$  such as:

$$\mathcal{B}_{ij} = -\frac{1}{2} \Omega^* \frac{C_{pq}}{2k} \frac{\Omega_p^* \Omega_q^*}{\Omega^{*2}} \left(R_{ij} - k \delta_{ij} + \frac{1}{2} C_{ij}\right) \quad (7)$$

The rotation also reduces the energy transfer from large to small turbulent scales. This phenomenon is modeled through an inverse flux  $J$  in the kinetic energy equation:

$$J = \frac{f_J}{1 + f_J} \varepsilon \quad (8)$$

where  $f_J$  is deduced from Aupoix's function (1987) and extended to the low-Reynolds number flow in order to vanish when  $\text{Re}_t$  goes to zero:

$$f_J = [1 - \exp(-\text{Re}_t^2)] \frac{0.12 \text{Ro}_t^{-2} + 0.015 \text{Ro}_t^{-1}}{0.254 \text{Ro}_t^{-2} + 0.157 \text{Ro}_t^{-1} + 1} \quad (9)$$

The corresponding term in the Reynolds stress equation is considered as isotropic for high Reynolds number and progressively approaches  $R_{ij}J/k$  as the Reynolds number diminishes:

$$J_{ij} = \frac{2}{3} (1 - f_T) \delta_{ij} J + f_T \frac{R_{ij}}{k} J \quad (10)$$

with the empirical function:

$$f_T = 1/(1 + \text{Re}_t/10)$$

In the rotating cavities, the effects of the inhomogeneity and of the shear are mixed with those of the rotation. To model these effects, we propose here an inhomogeneous term  $\mathcal{D}_{ij}$ , which can be written as:

$$\mathcal{D}_{ij} = 0.22 \left(\frac{k^2}{\varepsilon} \frac{2 \text{Ro}_t^{-1/2}}{1 + 15 \text{Ro}_t^{-1/2}} \frac{\Omega_i^* \Omega_m^*}{\Omega^{*2}} R_{ij,i}\right)_{,m} \quad (11)$$

The aim of this empirical term is also to take into account the significant increase of the turbulent diffusion (due to the triple fluctuating velocity correlation and to the fluctuating pressure) in the case of strong rotation (Shao et al. 1991).

The complete model is given in Table 2.

### Dissipation rate equation

Here we must recall the proposal of Launder and Tselepidakis (1994) for the dissipation rate equation, which is used for both the RSM2 and RSM3 models. The equation is sensitized to the Reynolds stress anisotropy through the destruction term of  $\varepsilon$ , and an empirical term is also introduced to represent the effects of pressure diffusion in the viscous sublayer:

$$\frac{d\varepsilon}{dt} = -c_{\varepsilon 1} \frac{\varepsilon}{k} R_{ij} U_{i,j} - c_{\varepsilon 2} \frac{\varepsilon \bar{\varepsilon}}{k} + \left(c_{\varepsilon} \frac{k}{\varepsilon} R_{ij} \varepsilon_{,j} + \nu \varepsilon_{,i}\right)_{,i}$$

$$+ c_{\varepsilon 3} \nu \frac{k}{\varepsilon} R_{jk} U_{i,jl} U_{i,kl} + \left(c_{\varepsilon 4} \nu \frac{\bar{\varepsilon}}{k} k_{,i}\right)_{,i} \quad (12)$$

**Table 2** RSM3 model for low Reynolds number flows

$$\frac{dR_{ij}}{dt} = P_{ij} + \phi_{ij}^{(1)} + \phi_{ij}^{(2)} + \phi_{ij}^{(2C)} + \phi_{ij}^{(2w)} + \phi_{ij}^{(2cw)} + D_{ij}^T + D_{ij}^v + \mathcal{D}_{ij} + \mathcal{B}_{ij} + J_{ij} - \varepsilon_{ij}$$

$P_{ij}, \phi_{ij}^{(1)}, \phi_{ij}^{(2)}, \phi_{ij}^{(2w)}, D_{ij}^T, D_{ij}^v$  and  $\varepsilon_{ij}$  have the same expression as in RSM2 model and:

$$\phi_{ij}^{(2C)} = -0.6 \left( D_{ij}^C - \frac{1}{3} D_{ij}^C \delta_{ij} \right) - 0.4k(U_{i,j} + U_{j,i})$$

$$\phi_{ij}^{(2cw)} = 0.2 \left( \phi_{km}^{(2C)} n_k n_m \delta_{ij} - \frac{3}{2} \phi_{ik}^{(2C)} n_k n_j - \frac{3}{2} \phi_{kj}^{(2C)} n_i n_k \right) \times \frac{k(R_{pq} n_p n_q)^{1/2}}{\varepsilon y}$$

$$\mathcal{D}_{ij} = 0.22 \left( \frac{k^2}{\varepsilon} f_{Ro} \frac{\Omega_k^* \Omega_j^*}{\Omega^{*2}} R_{ij,i} \right)_{,k}$$

$$\mathcal{B}_{ij} = -\alpha_{\mathcal{B}} (R_{ij} - k \delta_{ij} + \frac{1}{2} C_{ij})$$

$$J_{ij} = \left( f_T \frac{R_{ij}}{k} + \frac{2}{3} (1 - f_T) \delta_{ij} \right) J$$

$$C_{ij} = \frac{2}{3} \left( 1 + \frac{f_C}{2} \right) k \delta_{ij} - f_C k \frac{\Omega_i^* \Omega_j^*}{\Omega^{*2}}$$

$$J = \frac{f_J}{1 + f_J} \bar{\varepsilon}$$

$$f_T = \frac{1}{1 + Re_\tau/10}$$

$$f_J = [1 - \exp(-Re_\tau^2)] \frac{0.12 Ro_\tau^{-2} + 0.015 Ro_\tau^{-1}}{0.254 Ro_\tau^{-2} + 0.157 Ro_\tau^{-1} + 1}$$

$$f_{Ro} = \frac{2 Ro_\tau^{-1/2}}{1 + 15 Ro_\tau^{-1/2}} \quad \alpha_{\mathcal{B}} = \frac{1}{2} \Omega^* \frac{C_{pq} \Omega_p^* \Omega_q^*}{2k \Omega^{*2}}$$

$$f_C = \frac{Ro_\tau^{-1}}{5 + Ro_\tau^{-1}}$$

where  $\bar{\varepsilon} = \varepsilon - 2\nu k_{,i}^{1/2} k_{,i}^{1/2}$ ,  $c_\varepsilon = 0.18$ ,  $c_{\varepsilon 1} = 1.0$ ,  $c_{\varepsilon 2} = 1.92/(1 + 0.63(A.A_2^R)^{1/2})$ ,  $c_{\varepsilon 3} = 2.0$  and  $c_{\varepsilon 4} = 0.92$ .

For the RSM3 model, the inverse flux appears in the turbulent kinetic energy equation:

$$\begin{aligned} \frac{dk}{dt} = & -R_{ij} U_{i,j} + J - \varepsilon \\ & + 0.22 \left( \frac{k}{\varepsilon} R_{ij} k_{,j} + \nu k_{,i} \right)_{,i} \\ & + 0.22 \left( \frac{k^2}{\varepsilon} \frac{2 Ro_\tau^{-1/2}}{1 + 15 Ro_\tau^{-1/2}} \frac{\Omega_i^* \Omega_j^*}{\Omega^{*2}} k_{,i} \right)_{,j} \end{aligned} \quad (13)$$

and in an analogous way in the stress transport equation.

**Table 3** Characteristics of the employed meshes

Turbulence model	Number of points ( $N_z \times N_r$ )	$\Delta r/s$ at the upper wall	$\Delta z/s$ at the disks	Central cell, ( $\Delta z \times \Delta r$ )
$k - \varepsilon$ ASM				
and RSM1 models	80 × 100	4.0 × 10 <sup>-4</sup>	3.0 × 10 <sup>-4</sup>	0.03 × 0.15
RSM2 and RSM3 models	80 × 130	2.0 × 10 <sup>-4</sup>	3.0 × 10 <sup>-4</sup>	0.03 × 0.1

## Computational aspects

The numerical investigations has been done with a finite-volume code. The convection and diffusion terms are discretized with the power-law scheme and the velocity-pressure coupling is solved using the SIMPLER algorithm

To overcome the severe stability problems due to high rotation rates, several stabilizing techniques were introduced in the numerical procedure. Thus, the three velocity components are discretized on a staggered grid, but the turbulent stresses are all collocated at the pressure node allowing block solution, which strongly enhances stability. The 6 × 6 Reynolds stress system is solved by a direct method, which was necessary to reach the convergence. Several other stabilizing techniques were introduced in the code, such as an implicit treatment of Coriolis terms (Schiestel et al. 1993) (in the case of a rotating frame of reference) and regular and inertial relaxations. For implementation of the second-order closures, the code uses the decomposition  $R_{ij} = \Gamma_{(ij)} \partial U_i / \partial x_j + \sigma_{ij}$  introduced by Huang and Leschziner (1989), which allows us to restore a diffusive formulation for the Reynolds-stress terms in the mean flow equations. The complete procedure is described in Elena (1994) and Elena and Schiestel (1995b).

Use of low Reynolds number models requires use of thin grids near the walls in order to capture the rapid variations across the boundary layers. These are built according to geometrical series variations allowing a refinement near the walls. A grid independence study of the solution has been done, and the characteristics of the meshes used are given in Table 3. Because of numerous gradient terms, the RSM2 and RSM3 models need more discretization points in the center of the cavity than do the classical models.

## Discussion of the results

### Flow parameters

Figure 1 is a schematic diagram of the rotor-stator system considered, which is constituted of a rotating disk in a cylindrical casing. The dimensionless radius of the rotor is  $b/s = 12.5$ . The computations have been carried out with the five models for a rotational Reynolds number  $Re = 10^6$ , which corresponds to the experimental investigations of Itoh et al. For such a Reynolds number, the flow presents separated boundary layers on each disks. Then, the fluid moves radially outward along the rotor and returns inward along the stator. The motion is concentrated near the walls, and a central core is formed were the velocities are constant ( $U_\theta = Cte$  and  $U_r = U_z = 0$ ).

### Mean velocity profiles

The mean velocity profiles are given in Figures 2 and 3. They show, as in the experiment, that the radial flow is confined between the lateral walls and a nonviscous central region without any radial motion and where the tangential velocity is almost constant.

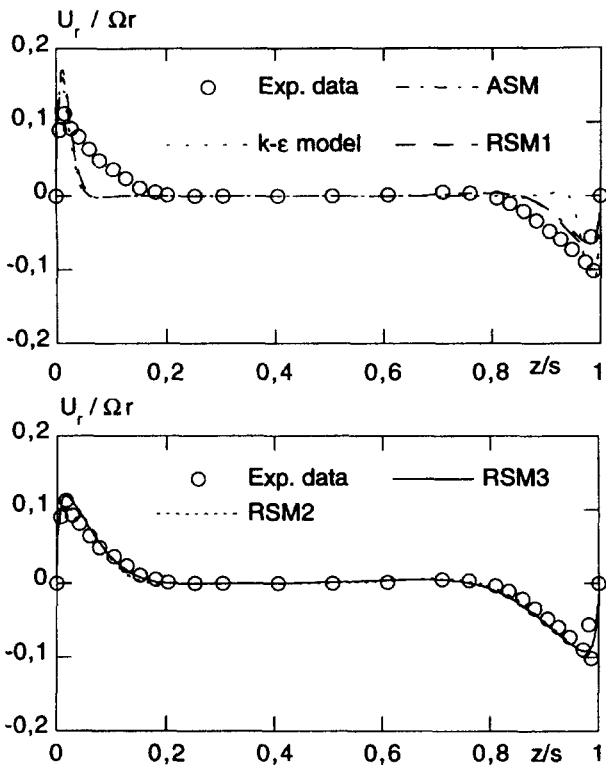


Figure 2 Radial velocity profiles,  $r/b=0.08$

The three classical models ( $k-\epsilon$  model, ASM, and RSM1) strongly underestimate the Ekman boundary-layer thickness on the rotor side. Indeed, these models provide an almost laminar flow near the rotor. A clear improvement is produced by the

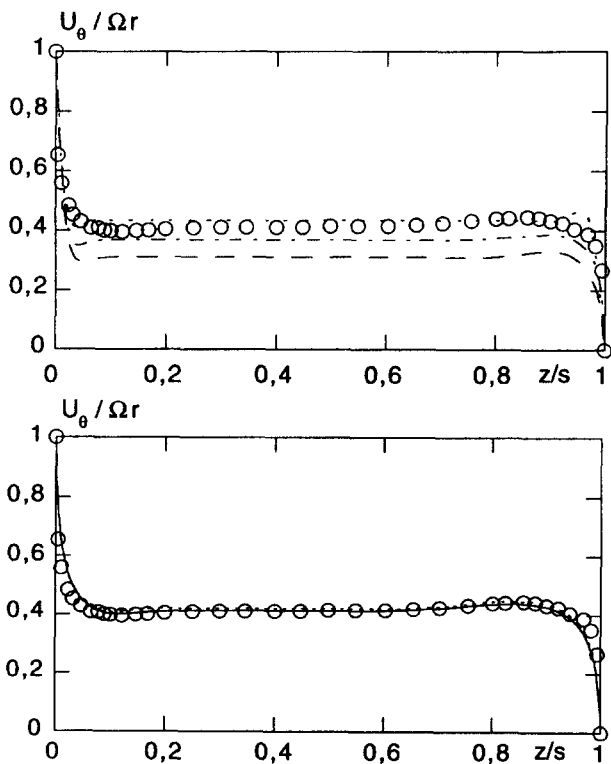


Figure 3 Tangential velocity profiles,  $r/b=0.8$  (same caption as Figure 2)

ASM and RSM1 models near the stator. The advanced models (RSM2 and RSM3) have a very satisfactory behaviour.

For the tangential velocity profiles (Figure 3) none of the classical models give, at once, a correct rotation rate of the central core and a satisfactory behaviour near the walls. Particularly, the local extrema that appear in the outer part of the boundary layers are characteristics of laminar flow. The RSM2 and RSM3 models both cure these weaknesses, and the computed profiles are then very close to the experimental one.

In fact, the Ekman layer thickness and the rotation rate of the central core directly depend on the flow regime. The classical models, which fail to predict the correct distribution of laminar and turbulent region, are then unable to produce a satisfactory description of the mean flow. The use of an advanced model seems to be necessary in order to compute the transition zone precisely.

Reynolds stress profiles

Figures 4 and 5 compare normal Reynolds stresses. Near the stator, the ASM model produces an acceptable distribution in the core region, but it deteriorates near the wall due to the wall region treatment based on  $k-\epsilon$ . The behaviour of the RSM1

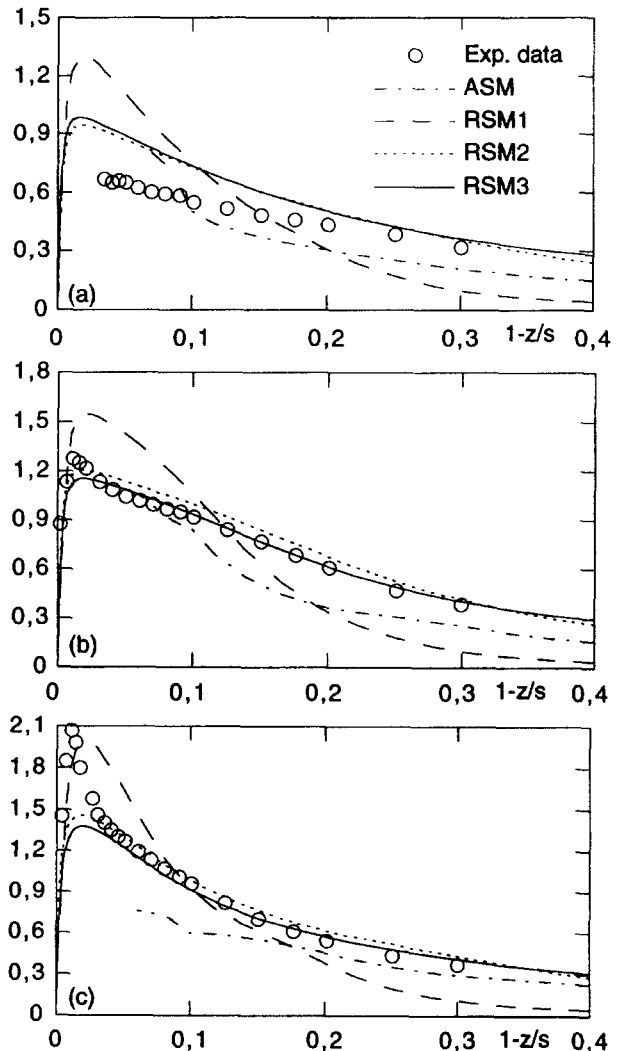


Figure 4 Reynolds stress profiles near the stator,  $r/b=0.8$ : (a),  $(R_{zz}/\tau_s)^{1/2}$ ; (b),  $(R_{rr}/\tau_s)^{1/2}$ ; (c),  $(R_{\theta\theta}/\tau_s)^{1/2}$

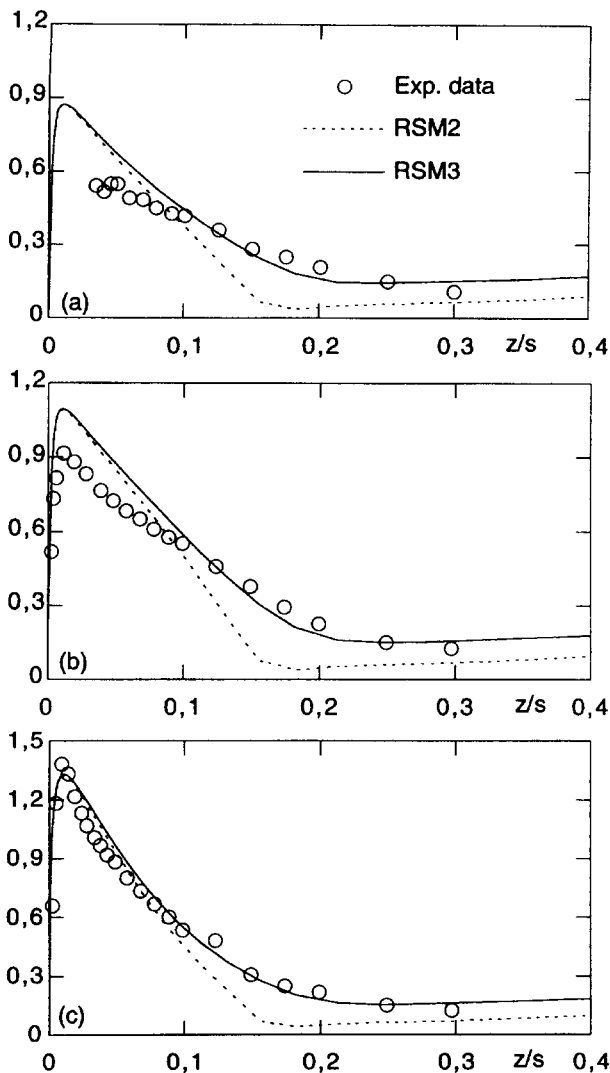


Figure 5 Reynolds stress profiles near the rotor,  $r/b=0.8$ : (a),  $(R_{zz}/\tau_r)^{1/2}$ ; (b),  $(R_{rr}/\tau_r)^{1/2}$ ; (c),  $(R_{\theta\theta}/\tau_r)^{1/2}$

model is unsatisfactory, with an overestimation of the maxima, and too strong an axial decrease. The results obtained with the RSM2 and RSM3 models are in satisfactory agreement with the experimental data, and the introduction of the new terms does not produce important changes in the predictions. However, a slight general improvement is given by the RSM3 model near the stator side. At the vicinity of the wall, the RSM2 and RSM3 models overestimate  $R_{zz}$  (which represents the fluctuations normal to the wall) and underestimate  $R_{\theta\theta}$ . This seems to show that the energy transfer between these two components is not completely accounted for by the models, and this is probably due to too crude a modeling of the wall reflection part of the pressure-strain correlation.

In the rotor boundary layer (Figure 5), only the results obtained with the RSM2 and RSM3 models are shown, the other models producing a relaminarized flow. The RSM2 model fails to mimic precisely the experimental stresses. Indeed, even if the maximum is well located, the axial decrease of the normal stress is too abrupt, leading to a quasirelaminarized flow in the core of the cavity. The modifications proposed here bring the Reynolds stress profiles into closer agreement with the experimental data.

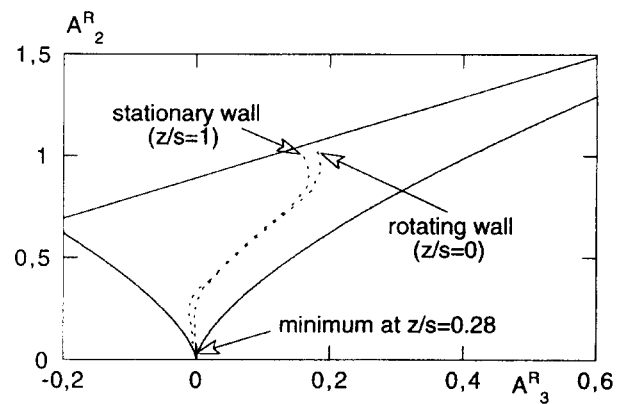


Figure 6 Reynolds stress tensor anisotropy, RSM3,  $r/b=0.8$

The slope of the Reynolds stress is then well predicted, and the turbulence level in the core of the cavity is in close agreement with the experimental one.

**Structure of the turbulent field**

Both confinement and rotation deeply affect the structure of turbulence but in a very different ways (Reynolds 1991).

- (1) *Two-component turbulence*: At the vicinity of a wall, the continuity requires that the fluctuations normal to the surface vanish faster than those parallel to it, and thus, the fluctuations lie in a plane parallel to the wall.
- (2) *Two-dimensional (2-D) turbulence*: The rotation has a tendency to produce long eddies aligned with the rotation axis, without variation along it (but the 2-D turbulence need not to be two-component).

Figures 6 and 7 emphasize that the RSM3 model captures well the structure of the turbulence submitted to the combined effects of rotation and confinement. On the invariant map of Figure 6, the second invariant of the Reynolds stress anisotropy,  $A_2^R$ , is plotted as a function of its third invariant  $A_3^R$ . It shows that the model respects the two-component limit near a solid boundary. The anisotropy diminishes as the distance to the wall increases, and in the central core of the flow, the turbulence is apparently quasi-isotropic.

The structural anisotropy based on the dimensionality tensor,  $a_{ij}^C = C_{ij}/k - 2/3\delta_{ij}$ , is given in Figure 7. The two invariant maps

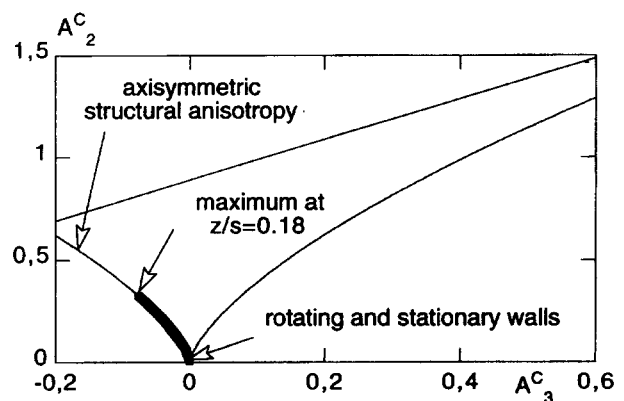


Figure 7 Dimensionality tensor anisotropy, RSM3,  $r/b=0.8$

are bounded by the curve  $A_3^C = -A_2^{C3/2}/\sqrt{6}$ , which represents a structural axisymmetric behaviour. In the core of the flow, the structural anisotropy is high, which may be interpreted as the presence of "cylindrical" eddies aligned with the rotation axis. Near the lateral walls, the anisotropy is strongly damped. The turbulent structures do not have a privileged direction: the "cylindrical" eddies are then destroyed by the wall and the shear in the boundary layer.

The very different meaning of the two anisotropies is emphasized by these two diagrams. The Reynolds stress anisotropy provides only componentality informations, which the structural anisotropy describes the dimensionality of turbulence in the sense of the Reynolds (1991) approach.

## Conclusion

Five models were applied to the prediction of the turbulent flow inside a shrouded rotor-stator system. The following conclusions may be drawn from this numerical study:

- (1) Classical models such as the  $k-\varepsilon$  model and the "old fashioned" Reynolds stress model do not provide a correct location of the relaminarized and turbulent regions. Thus, the Ekman layer thickness and the tangential velocity of the central core are not well predicted.
- (2) A zonal modeling with a high Reynolds number model in the core of the flow and a low Reynolds number one for wall treatment is not well adapted to this type of flow. Indeed, a relaminarized region extends away from the wall.
- (3) The differential stress models of the new generation proved to be an adequate level of closure in order to study so complex a flow. The model chosen well predicts the mean velocity and Reynolds stress near the stationary wall. However, the model is not able to capture the strong effects of rotation on the turbulence and therefore, the Reynolds stresses near the rotor are unsatisfactory.
- (4) The present proposals that take into account the implicit effects of the rotation on the nonhomogeneous turbulence field were shown to cure the main failures of the classical models and constitute a promising way to predict inhomogeneous turbulent flow submitted to rapid rotation. Further investigations for various flows conditions are necessary to test the degree of universality of the model.

## Acknowledgments

The computations were carried out on the Cray YMP-2E computer of the Institut Méditerranéen de Technologie (Marseille) with support of DRET (group 6) and SNECMA (YKL group); they are here gratefully acknowledged.

## References

- Aupoix, B. 1987. Application de modèles dans l'espace spectral à d'autres niveaux de fermeture en turbulence homogène. Thèse Doct Es Sc., Univ. de Lyon
- Cambon, C., Jacquin, L. and Lubrano, J. L. 1992. Towards a new Reynolds-stress model for rotating turbulent flow. *Phys. Fluids, A*, **4**, 812-824
- Craft, T. J. 1991. Second-moment modelling of turbulent scalar transport, Ph.D. thesis, Faculty of Technology, University of Manchester, Manchester, UK
- Elena, L. 1994. Modélisation de la turbulence inhomogène en présence de rotation. Thèse de Doctorat, Univ. d'Aix-Marseille II
- Elena, L. and Schiestel, R. 1995a. Turbulence modeling of confined flow in rotating disc systems. *AIAA J.*, **33**, 812-821
- Elena, L. and Schiestel R. 1995b. Résolution numérique des équations de transport des tensions de Reynolds en écoulements turbulents tournants en milieu confiné. *Revue Européenne des Eléments Finis* **4**, 7-32
- Hanjalic K. and Launder, B. E. 1976. Contribution towards a Reynolds-stress closure for low-Reynolds number turbulence. *J. Fluid Mech.*, **74**, 583-610
- Huang, P. G. and Leschziner, M. A. 1989. Stabilization of recirculating flow computations performed with second-moment closures and third-order discretization. *Proc. 5th Int. Symposium of Turbulent Shear Flow*, Cornell University, Ithaca, NY
- Itoh, M., Yamada Y., Imao S. and Gonda, M. 1990. Experiments on turbulent flow due to an enclosed rotating disk. In *Proc. Int. Symposium on Engineering Turb. Modelling, and Experiments*, Dubrovnik, Yugoslavia, W. Rodi and E. N. Ganić (eds.), Elsevier Science, New York, 659-668
- Launder, B. E. and Reynolds, W. C. 1983. Asymptotic near-wall stress dissipation rates in a turbulent flow. *Phys. Fluids A*, **26**, 1157
- Launder, B. E. and Sharma, B. I. 1974. Application of the energy-dissipation model of turbulence to the calculation of flow near a spinning disk. *Lett. Heat Mass Transfer*, **1**, 131-138
- Launder B. E. and Tselepidakis, D. P. 1994. Application of a new second-moment closure to turbulent channel flow rotating in orthogonal mode. *Int. J. Heat Fluid Flow*, **15**, 2-10
- Reynolds, W. C. 1991. Towards a structure-based turbulence model. In *Studies in Turbulence*, T. B. Gatski, S. Sarkar and C. G. Speziale (eds.), Springer, New York, 1-15
- Reynolds, W. C. and Kassinos, S. C. 1994. A one-point model for the evolution of the Reynolds stress and structure tensors in rapidly deformed homogeneous turbulence. *Proc. Osborne Reynolds Centenary Symposium*, UMIST, Manchester, UK
- Schiestel, R. 1994. Quelques concepts pour la modélisation des écoulements turbulents confinés en rotation. Note IM2, no 94/1, Univ. d'Aix-Marseille II
- Schiestel R., Elena L. and Rezoug, T. 1993. Numerical modelling of turbulent flow and heat transfer in rotating cavities. *Num. Heat Transfer A*, **24**, 45-65
- Shao, L., Michard, M. and Bertoglio, J-P. 1991. Effects of solid body rotation on the transport of turbulence. *Proc. 8th Symposium of Turbulent Shear Flows*, Munich, Germany. Paper 30-5